Angular momentum of fission fragments in low energy fission of actinides

H. Naik, S. P. Dange, and R. J. Singh
Radiochemistry Division, Bhabha Atomic Research Centre, Trombay, Mumbai-400 085, India
(Received 4 August 2003; published 11 January 2005)

Independent isomeric yield ratios (IYR) of ^{128}Sb, ^{130}Sb, ^{132}Sb, ^{131}Te, ^{133}Te, ^{132}I, ^{134}I, ^{136}I, ^{135}Xe, and ^{138}Cs have been determined in fast neutron induced fission of ^{232}Th, ^{238}U, ^{240}Pu, and ^{244}Cm as well as in thermal neutron induced fission of ^{232}U and ^{238}Pu using radiochemical and offline γ-ray spectrometric techniques. From the IYR, fragment angular momenta ($J_{\rm rms}$) have been deduced using a spin-dependent statistical model analysis. These data along with the literature data for ^{230}Th*, ^{234}U*, ^{236}U*, ^{240}Pu*, ^{242}Pu*, ^{244}Cm(SF), ^{246}Cm*, ^{250}Cf*, and ^{252}Cf(SF) for fifteen even-Z fissioning systems show the following important features: (i) The $J_{\rm rms}$ of the odd-Z fission products are higher than those of the even-Z fission products, indicating the odd-even effect. For both the odd-Z and even-Z fission products, the $J_{\rm rms}$ increase with Z_F^2/A_F. (ii) The $J_{\rm rms}$ of fragments with spherical 50-p and 82-n shells are lower compared to those of fragments outside the spherical shell, indicating the effect of shell closure proximity. (iii) The $J_{\rm rms}$ of the fission products increase with mass number in spite of fluctuations in shell closure proximity and odd-even effects but do not show any correlation with the neutron emission curve. (iv) In all fifteen even-Z fissioning systems from Th to Cf, the yield-weighted $J_{\rm rms}$ values show an anticorrelation with the elemental yields. (v) The odd-even fluctuation on $J_{\rm rms}$ does not change drastically from Th to Cf, unlike the proton odd-even effect (δ_p) which decreases significantly with the increase of Coulomb parameter ($Z_F^2/A_F^{1/3}$).

DOI: 10.1103/PhysRevC.71.014304 PACS number(s): 25.85.−w

I. INTRODUCTION

Fission fragment angular momentum in low energy fission of actinides arises due to statistical populations in various collective modes such as wriggling, bending, and twisting [1,2] in addition to the contribution from postscission Coulomb torque [2–4] and/or single particle excitation. Thus, studies on the fragment angular momentum are of theoretical and experimental interest as they provide information about the rotational degrees of freedom at the point of scission and shortly after scission. Fragment angular momentum of the mass average fission products can be estimated from the physical methods based on measurements of anisotropy [3,4] and multiplicity [5,6] of the prompt γ rays. For even-even fission products, fragment angular momentum can be estimated from their ground-state rotational band transition intensity, measured by using the multiparameter coincidence technique [7,8] and applying statistical model analysis. On the other hand, fragment angular momenta of both even-Z and odd-Z fission products can be estimated from the independent isomeric yield ratios [9–22] using statistical model analysis. Depending upon the half-lives of the radionuclides, the independent isomeric yield ratios of the fission products are determined using the physical techniques based on a recoil mass separator [9–11], an isotope separator, or the ISOL [12], or by radiochemical methods [13–22]. The physical technique based on a recoil mass separator [9–11] provides the fragment angular momentum of the fission product as a function of fragment kinetic energy. On the other hand, in the radiochemical method combined with offline γ-ray spectrometry it is possible to obtain the angular momentum of the fission product for the integral over the kinetic energy. Studies on fragment angular momentum based on the above techniques may reveal dependencies on nuclear structure effects such as odd-even effects [17–22], shell closure proximity [17–22], quadrupole moments [7], scission point deformation [8,20–22], fragment kinetic energy [9–12], and the single particle effect of the fissioning systems [22]. An anticorrelation of fragment angular momentum with elemental yield was also observed in the even-Z fissioning systems [20,21] due to the coupling between the collective and intrinsic degrees of freedom. The observed trend of decreasing angular momentum with increasing kinetic energy [9–11] for different fragments also confirms this fact as well as the effect of fragment deformation. The observation of the odd-even effects on fragment angular momentum in the odd-Z fissioning systems [22] further supports the role of fragment deformation in addition to the single particle spin contribution of the fission fragments and the fissioning systems. All of the above observations are based on the data in the even-even and odd-odd fissioning systems except the data for ^{133}Xe and ^{135}Xe in ^{238}U(n_f, f) and ^{242}Am^m($n_{\rm th}$, f) [16]. Thus it seems that the data in the even-odd and odd-even fissioning systems are extremely rare. In view of this, in the present work fragment angular momenta of ^{128}Sb, ^{130}Sb, ^{132}Sb, ^{131}Te, ^{133}Te, ^{132}I, ^{134}I, ^{136}I, ^{135}Xe, and ^{138}Cs have been deduced from the radiochemically determined independent isomeric yield ratios in fast neutron induced fission of ^{232}Th, ^{238}U, ^{240}Pu, and ^{244}Cm as well as in thermal neutron induced fission of ^{232}U and ^{238}Pu, respectively. These data in the even-odd fissioning systems and the literature data of even-even and odd-odd fissioning systems are interpreted in terms of various aspects of the fission fragment on its angular momentum, such as the effect of mass, charge, and shell closure proximity. The single particle (proton or neutron) spin effect of the fissioning system on fragment angular momentum is also discussed.

II. EXPERIMENTAL PROCEDURES

For thermal neutron induced fission, 100 μl of the nitrate solutions of ^{232}U (10.0 μg/ml) and ^{238}Pu (50.0 μg/ml) were

put in polypropylene tubes and doubly sealed in alkathene bags. They were then irradiated in the reactor APSARA for 3 to 60 min at a flux of $1.2 \times 10^{12}\, n\ \mathrm{cm}^{-2}\ \mathrm{s}^{-1}$. In the case of fast neutron induced fission, a known amount of 25-μm-thick ^{232}Th metal foil ($\sim$50 mg) and electrodeposited targets of 99.9997 atom % ^{238}U ($\sim$500 μg), 99.48 atom % ^{240}Pu (96 μg), and 99.43 atom % ^{244}Cm (96 μg) were covered with 75-μm-thick Lexan foil or 25-μm-thick aluminum foil which acted as a catcher to collect the fission products during the neutron irradiation of the target. They were then wrapped with 1-mm-thick cadmium foil, doubly sealed in alkathene bags and irradiated for 5 to 60 min in the same irradiation position of the reactor APSARA. In the case of ^{238}U, ^{240}Pu, and ^{244}Cm, after the irradiation, the aluminum catcher foils were dissolved in dilute sodium hydroxide solution, and iodine was separated using standard radiochemical procedures [23]. On the other hand, the Lexan catcher foils were washed with very dilute nitric acid solutions followed by distilled water for removing the possible contamination of activation products from ^{232}Th and ^{238}U, and the alpha contamination of ^{240}Pu and ^{244}Cm. The irradiated targets of sealed polypropylene tubes for ^{232}U and ^{238}Pu as well as the Lexan catcher foils in the case of ^{232}Th, ^{238}U, ^{240}Pu, and ^{244}Cm were then mounted on perspex plates, whereas the standard aliquots of the separated iodine samples were taken in the counting vials. The samples were then counted in a fixed geometry on an energy- and efficiency-calibrated 120-c.c. HPGe detector coupled to a PC-based 4096-channel analyzer. The resolution of the detector system was 1.8 keV at 1332.0 keV of ^{60}Co. In the case of ^{232}Th, ^{238}U, ^{240}Pu, and ^{244}Cm, from the above type of irradiation it is possible for inert gas fission products such as krypton and xenon to escape. To prevent the escape of inert gaseous fission products and to better assess the short-lived fission products, $\sim$10 mg of ^{232}Th metal foil, $\sim$5 mg of ^{238}U oxide, and $\sim$200 μl each of ^{240}Pu (0.507 mg/ml) and ^{244}Cm (0.55 mg/ml) in the form of nitrate solutions were sealed in polypropylene tubes. They were then covered with 1-mm-thick cadmium foils, doubly sealed in alkathene bags, and irradiated for 2 to 5 min using the pneumatic carrier facility of the reactor CIRUS at a flux of $5.0 \times 10^{12}\, n\ \mathrm{cm}^{-2}\ \mathrm{s}^{-1}$. The irradiated targets were mounted as such on the perspex plates without opening the tubes. They were then analyzed by γ-ray spectrometry at a fixed geometry in an energy- and efficiency-calibrated 80-c.c. HPGe detector coupled to a PC-based 4096-channel analyzer. The resolution of the detector system was 2.0 keV at 1332.0 keV of ^{60}Co. The dead time was always less than 10% to avoid the pileup effect. The γ-ray counting of the samples was done in real time and was followed as a function of time for at least three half-lives. The γ lines and the nuclear spectroscopic data of different nuclides used in the present work were taken from Refs. [24], and [25]. From the photopeak areas of γ lines of the nuclides, independent isomeric yields were determined using usual decay-growth equations [15–22] after correcting for the precursor contribution. The cumulative yields and the fractional cumulative yields of the precursors were taken from either the literature [26–32] or our recent work [33,34]. The activities of ^{92}Sr and ^{104}Tc in the unseparated samples irradiated for either a long time or a short time and of ^{135}I in the separated iodine samples were used as fission rate monitors. The independent isomeric yield ratios determined in the present work are for ^{128}Sb, ^{130}Sb, ^{132}Sb, ^{131}Te, ^{133}Te, ^{132}I, ^{134}I, ^{136}I, ^{135}Xe, and ^{138}Cs in fast neutron induced fission of ^{232}Th, ^{238}U, ^{240}Pu, and ^{244}Cm, as well as in thermal neutron induced fission of ^{232}U and ^{238}Pu, respectively. Among these, independent isomeric yields of some of the fission products such as those for ^{128}Sb, ^{131}Te, ^{134}I, and ^{136}I in ^{232}Th(n_f, f) [26,28]; ^{134}I and ^{135}Xe in ^{238}U(n_f, f) [16,29]; ^{130}Sb, ^{134}I, ^{135}Xe, and ^{138}Cs in ^{232}U(n_{th}, f) [31]; and ^{130}Sb, ^{133}Te, ^{135}Xe, and ^{138}Cs in ^{238}Pu(n_{th}, f) [32] were calculated from the literature data of independent/cumulative yields of the isomers and using charge distribution systematics [33–36].

III. RESULTS AND DISCUSSION

The independent isomeric yield ratios (IYR) of various fission products (e.g., ^{128}Sb, ^{130}Sb, ^{132}Sb, ^{131}Te, ^{133}Te, ^{132}I, ^{134}I, ^{136}I, ^{135}Xe, and ^{138}Cs) in fast neutron induced fission of ^{232}Th, ^{238}U, ^{240}Pu, and ^{244}Cm as well as in thermal neutron induced fission of ^{232}U and ^{238}Pu determined in the present work and/or from the literature [16,26–32] are given in Table I. The uncertainties for the isomeric yield ratios include the errors due to the counting statistics, absolute abundances of the γ lines, detector efficiencies, the fission yields of the precursors, and the least-squares analysis. In the fissioning systems ^{241}Pu* and ^{245}Cm*, all the data are determined for the first time. In the other four fissioning systems some of the data are determined for the first time except for ^{128}Sb, ^{132}Sb, ^{134}I, and ^{136}I in ^{233}Th* [26–28] and for ^{134}I and ^{135}Xe in ^{239}U* [16,29]. The IYR for ^{130}Sb, ^{134}I, ^{135}Xe, and ^{138}Cs in ^{233}U* as well as for ^{130}Sb, ^{133}Te, ^{135}Xe, and ^{138}Cs in ^{239}Pu* from the present work are seen to be in close agreement with the values deduced from the literature data [31–36]. From the isomeric yield ratios (IYR), the fragment angular momenta (J_{rms}) were deduced using spin-dependent statistical model analysis [37] as reported earlier [18–22], and they are also given in Table I. The yield-weighted average angular momenta of various elements in the above-mentioned fissioning systems and for other even-Z fissioning systems from the earlier work [20,21] are given in Table II. The present data for the even-odd fissioning systems are compared with similar data for even-even [20,21] and odd-odd [22] fissioning systems.

A. Effect of nuclear structure and scission-point deformation on fragment angular momentum

The yield-weighted fragment angular momenta (J_{rms}) of the adjacent elements in fifteen different even-Z fissioning systems from Table II are plotted in Fig. 1 as a function of the atomic number. Furthermore J_{rms} of various isotopes of different elements such as antimony, tellurium, iodine, and xenon from the present work for even-odd fissioning systems along with similar data for even-even, odd-odd, and odd-even fissioning systems from the literature [7–22] are plotted in Fig. 2 as a function of fissility parameter (Z_F^2/A_F). Error bars are not shown in the figure, because their inclusion would make the figure difficult to read. From Fig. 1 it can be seen that in all

TABLE I. Independent isomeric yield ratio, fragment J_{rms}, and various parameters related to scission-point configuration in the fissioning systems ^{233}Th*, ^{233}U*, ^{239}U*, ^{239}Pu*, ^{241}Pu*, and ^{245}Cm*.

Nuclide	$IY(\%)$	$Y_h/(Y_h+Y_l)$	Ref.[b]	J_{rms}	β	C	T	KE (MeV)	
	(Y_h+Y_l)[a]		($\hbar$)			(fm)	(MeV)	Exp.	Cal.
^{233}Th*									
^{128}Sb	0.0056 ± 0.0014	0.537 ± 0.146	26	10.5 ± 2.5	0.80	1.06	0.75	170.8	171.2
^{130}Sb	0.163 ± 0.072	0.490 ± 0.150	A	9.8 ± 2.0	0.63	1.04	0.75	168.8	168.0
^{132}Sb	0.961 ± 0.038	0.387 ± 0.056	A	7.7 ± 0.8	0.40	1.05	0.71	169.7	169.6
^{131}Te	0.028 ± 0.008	0.621 ± 0.050	26	5.1 ± 0.6	0.04	1.06	0.69	170.4	170.7
^{133}Te	1.543 ± 0.147	0.560 ± 0.063	A	4.6 ± 0.7	0.001	1.14	0.61	170.3	183.6
^{134}I	0.086 ± 0.021	0.470 ± 0.050	28	8.7 ± 0.5	0.41	1.06	0.70	169.0	170.0
^{136}I	1.880 ± 0.346	0.710 ± 0.050	28	8.9 ± 0.9	0.39	1.03	0.71	165.7	165.2
^{135}Xe	0.116 ± 0.022	0.565 ± 0.109	A	4.7 ± 1.0	0.011	1.13	0.61	167.0	180.5
^{138}Cs	1.016 ± 0.149	0.658 ± 0.119	A	9.0 ± 1.7	0.41	1.03	0.71	163.3	163.7
^{233}U*									
^{128}Sb	0.336 ± 0.022	0.537 ± 0.060	A	10.5 ± 1.0	0.80	1.06	0.75	176.7	177.3
^{130}Sb	1.747 ± 0.122	0.427 ± 0.055	A	8.8 ± 0.9	0.45	1.06	0.72	177.0	177.3
	1.791 ± 0.107	0.440 ± 0.040	31	9.1 ± 0.6	0.51	1.07	0.72	177.0	177.3
^{132}Sb	1.369 ± 0.070	0.381 ± 0.028	A	7.7 ± 0.3	0.20	1.07	0.68	178.0	179.0
^{131}Te	1.499 ± 0.165	0.676 ± 0.068	A	5.8 ± 1.0	0.22	1.07	0.69	179.0	177.5
^{133}Te	3.833 ± 0.050	0.579 ± 0.013	A	4.8 ± 0.2	0.001	1.10	0.64	177.3	183.5
^{132}I	0.371 ± 0.041	0.456 ± 0.076	A	8.6 ± 1.0	0.41	1.07	0.70	178.0	177.9
^{134}I	2.320 ± 0.328	0.394 ± 0.063	A	7.8 ± 0.8	0.20	1.06	0.68	176.0	176.3
	2.420 ± 0.050	0.443 ± 0.061	31	8.4 ± 0.8	0.34	1.06	0.69	176.0	176.3
^{135}Xe	1.670 ± 0.160	0.621 ± 0.062	A	5.2 ± 0.7	0.05	1.06	0.66	174.8	175.6
	1.670 ± 0.280	0.595 ± 0.058	31	4.9 ± 0.6	0.001	1.08	0.64	174.8	178.9
^{138}Cs	2.005 ± 0.156	0.693 ± 0.110	A	9.7 ± 1.7	0.57	1.04	0.71	172.0	171.6
	1.110 ± 0.030	0.676 ± 0.153	31	9.3 ± 2.1	0.48	1.04	0.70	172.0	171.6
^{239}U*									
^{128}Sb	0.049 ± 0.005	0.517 ± 0.094	A	10.2 ± 1.5	0.76	1.07	0.74	176.0	176.9
^{130}Sb	0.866 ± 0.043	0.431 ± 0.051	A	8.9 ± 0.7	0.50	1.08	0.70	178.0	178.6
^{132}Sb	3.031 ± 0.345	0.310 ± 0.058	A	6.8 ± 0.7	0.24	1.08	0.68	178.5	178.6
^{131}Te	0.145 ± 0.007	0.651 ± 0.072	A	5.5 ± 0.9	0.16	1.08	0.67	177.0	178.1
^{133}Te	2.910 ± 0.180	0.561 ± 0.061	A	4.7 ± 0.7	0.001	1.12	0.62	177.5	184.1
^{132}I	0.018 ± 0.005	0.460 ± 0.026	A	8.7 ± 0.3	0.45	1.08	0.69	178.5	179.2
^{134}I	0.989 ± 0.064	0.397 ± 0.033	29	7.8 ± 0.4	0.23	1.08	0.67	177.5	177.6
^{136}I	2.992 ± 0.503	0.678 ± 0.092	A	8.3 ± 1.5	0.32	1.07	0.68	175.0	175.9
^{135}Xe	0.089 ± 0.005	0.629 ± 0.066	16	5.3 ± 0.7	0.08	1.07	0.66	175.0	175.3
^{138}Cs	0.058 ± 0.042	0.680 ± 0.023	A	9.2 ± 0.6	0.50	1.06	0.69	172.5	172.9
^{239}Pu*									
^{128}Sb	0.201 ± 0.035	0.524 ± 0.128	A	10.3 ± 1.7	0.75	1.05	0.75	179.5	179.5
^{130}Sb	1.649 ± 0.144	0.447 ± 0.039	A	9.2 ± 0.6	0.55	1.07	0.71	183.0	183.0
	1.748 ± 0.194	0.493 ± 0.090	32	9.9 ± 1.3	0.70	1.07	0.72	173.0	183.0
^{132}Sb	1.307 ± 0.077	0.358 ± 0.038	A	7.4 ± 0.5	0.38	1.08	0.69	184.0	184.7
^{131}Te	2.544 ± 0.147	0.660 ± 0.040	A	5.6 ± 0.5	0.19	1.08	0.67	184.5	184.3
^{133}Te	5.637 ± 0.262	0.562 ± 0.040	A	4.6 ± 0.4	0.001	1.14	0.61	184.5	194.5
	5.405 ± 0.224	0.541 ± 0.033	32	4.4 ± 0.3	0.001	1.18	0.58	184.5	201.4
^{132}I	0.452 ± 0.032	0.455 ± 0.043	A	8.6 ± 0.6	0.43	1.08	0.69	184.0	183.8
^{134}I	3.330 ± 0.150	0.380 ± 0.061	A	7.7 ± 0.8	0.21	1.08	0.67	183.3	183.8
^{136}I	2.427 ± 0.212	0.711 ± 0.084	A	8.9 ± 1.4	0.46	1.07	0.69	181.5	182.1
^{135}Xe	2.163 ± 0.208	0.591 ± 0.059	A	4.8 ± 0.6	0.001	1.10	0.63	182.8	186.7
	2.559 ± 0.235	0.655 ± 0.073	32	5.5 ± 0.9	0.15	1.08	0.66	182.8	183.3
^{138}Cs	1.990 ± 0.035	0.666 ± 0.076	A	9.1 ± 1.4	0.47	1.06	0.69	179.0	179.3
	1.380 ± 0.030	0.723 ± 0.073	32	10.4 ± 1.3	0.74	1.06	0.70	179.0	179.3

[a] Y_h and Y_l = Yield of high- and low-spin isomers.
[b] A = Data are from the present work.

TABLE I. (*Continued*.)

Nuclide	$IY(\%)$ $(Y_h + Y_l)$[a]	$Y_h/(Y_h + Y_l)$	Ref.[b]	$J_{\rm rms}$	β	C	T	KE (MeV)	
			($\hbar$)			(fm)	(MeV)	Exp.	Cal.
^{241}Pu*									
^{128}Sb	0.245 ± 0.014	0.505 ± 0.032	A	10.0 ± 0.9	0.72	1.07	0.73	182.8	182.3
^{130}Sb	1.501 ± 0.251	0.446 ± 0.123	A	9.1 ± 1.5	0.57	1.09	0.70	186.3	185.7
^{132}Sb	2.260 ± 0.019	0.321 ± 0.007	A	7.5 ± 0.2	0.19	1.10	0.66	187.0	187.4
^{131}Te	1.300 ± 0.119	0.656 ± 0.117	A	5.5 ± 0.7	0.19	1.10	0.66	187.0	187.0
^{133}Te	3.024 ± 0.132	0.593 ± 0.095	A	4.9 ± 0.9	0.05	1.10	0.64	187.0	187.0
^{132}I	0.195 ± 0.020	0.440 ± 0.080	A	8.4 ± 0.9	0.41	1.10	0.67	187.0	186.5
^{134}I	3.529 ± 0.162	0.396 ± 0.028	A	7.8 ± 0.4	0.26	1.10	0.65	186.6	186.5
^{136}I	3.002 ± 0.008	0.654 ± 0.087	A	8.0 ± 1.5	0.28	1.09	0.66	184.0	184.9
^{135}Xe	0.755 ± 0.080	0.697 ± 0.077	A	4.95 ± 0.85	0.04	1.10	0.63	185.4	186.0
^{138}Cs	1.343 ± 0.103	0.679 ± 0.040	A	9.5 ± 0.8	0.58	1.07	0.69	180.8	180.3
^{245}Cm*									
^{128}Sb	0.422 ± 0.023	0.540 ± 0.036	A	10.6 ± 0.6	0.91	1.11	0.71	193.5	193.8
^{130}Sb	1.241 ± 0.142	0.511 ± 0.067	A	10.0 ± 0.9	0.79	1.12	0.69	195.5	195.6
^{132}Sb	1.469 ± 0.212	0.332 ± 0.057	A	7.1 ± 0.6	0.26	1.11	0.65	194.0	193.8
^{131}Te	1.447 ± 0.199	0.654 ± 0.142	A	5.4 ± 1.5	0.20	1.12	0.64	195.5	195.3
^{133}Te	2.968 ± 0.374	0.595 ± 0.040	A	4.9 ± 0.4	0.05	1.11	0.63	194.0	195.3
^{132}I	0.547 ± 0.027	0.486 ± 0.067	A	8.9 ± 0.8	0.77	1.12	0.68	195.0	194.9
^{134}I	1.964 ± 0.202	0.410 ± 0.059	A	8.4 ± 0.9	0.42	1.11	0.66	193.0	193.5
^{136}I	3.869 ± 0.029	0.749 ± 0.067	A	9.8 ± 1.4	0.70	1.10	0.68	191.0	191.4
^{135}Xe	1.606 ± 0.284	0.681 ± 0.078	A	5.8 ± 0.9	0.25	1.10	0.65	191.5	191.0
^{138}Cs	2.096 ± 0.208	0.694 ± 0.099	A	9.7 ± 1.7	0.65	1.08	0.67	188.5	188.7

[a]Data are from Ref. [21].
[b]Data are from the present work.

fifteen even-Z fissioning systems the $J_{\rm rms}$ of odd-Z elements are higher than those of their neighboring even-Z elements. A similar observation was also made in earlier work [22] for the odd-Z fissioning systems. This indicates the odd-even effect on fragment angular momentum. The higher angular momentum of odd-Z elements may be due to fragment single particle effects or to the higher deformation of the odd-Z fragment resulting from the polarization of the even-Z core by the odd proton, as indicated by Madsen and Brown [38]. On the other hand, from Fig. 2 it can be seen that the $J_{\rm rms}$ of both even-Z and odd-Z fragments show a trend of increasing with Z_F^2/A_F. This may be due to the increase in the Coulomb torque with Z_F^2/A_F.

TABLE II. Yield-weighted average fragment angular momenta of heavy mass elements in the fifteen different even-Z fissioning systems.

Nuclide	In	Sn	Sb	Te	I	Xe	Cs	Ba	Ce	Nd	Pm	Sm
^{230}Th*[a]	-	-	7.49	4.76	8.11	4.7	8.7	-	-	-	-	-
^{233}Th*[b]	-	-	8.02	4.61	8.89	4.7	9.0	-	-	-	-	-
^{233}U*[b]	-	-	8.67	5.08	7.87	5.05	9.5	-	-	-	-	-
^{234}U*[a]	-	-	7.74	4.93	8.01	4.86	10.1	-	-	-	11.8	-
^{236}U*[a]	6.76	5.7	6.77	4.98	8.15	5.5	10.0	-	-	-	11.0	-
^{239}U*[b]	-	-	7.28	4.73	8.2	5.3	9.2	-	-	-	-	-
^{239}Pu*[b]	-	-	8.72	4.83	8.33	5.15	9.1	-	-	-	-	-
^{240}Pu*[a]	-	-	8.27	5.27	8.45	5.13	9.35	-	-	-	-	-
^{241}Pu*[b]	-	-	7.86	5.08	7.91	4.95	9.5	-	-	-	-	-
^{242}Pu*[a]	-	-	6.53	4.38	8.12	5.45	8.9	-	-	-	-	-
^{244}Cm[c]	-	-	8.49	4.87	8.7	5.8	8.7	-	-	-	-	-
^{245}Cm*[b]	-	-	8.61	5.06	9.24	5.8	9.7	-	-	-	-	-
^{246}Cm*[a]	-	-	9.03	4.96	8.53	5.85	8.9	-	-	-	-	-
^{250}Cf*[a]	-	-	12.35	5.69	8.4	6.4	9.3	-	-	-	9.7	-
^{252}Cf[a]	-	-	8.06	4.55	9.97	7.83	7.9	7.24	8.87	9.39	-	11.1

[a]Data are from Ref. [21].
[b]Data are from the present work.
[c]Data are from Ref. [20].

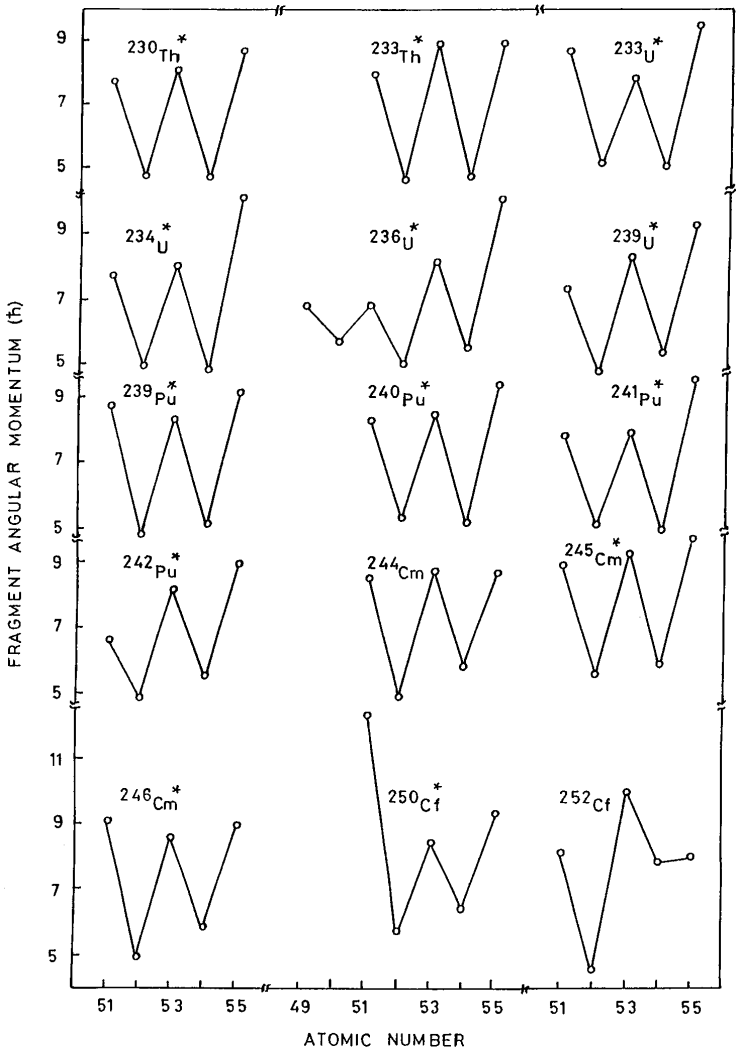

FIG. 1. The plot of yield-weighted average fragment angular momenta as a function of the atomic number of various elements in fifteen different even-Z fissioning systems.

It can also be seen from Fig. 2 that the $J_{\rm rms}$ of ^{132}Sb, ^{133}Te, ^{134}I, and ^{135}Xe are lower than those of ^{128,130}Sb, ^{131,132}Te, ^{132,136}I, and ^{133,138}Xe, respectively. This may be due to the presence of the spherical 82-n shell in the fragments corresponding to the former products, if one considers one neutron emission in this mass region. This indicates the effect of shell closure proximity [20–22]. The effect of shell closure configuration is also evident from the higher $J_{\rm rms}$ of fission products having a deformed 66-n or 88-n shell in their fragment stage in the spontaneous fission of ^{252}Cf [7,20,21]. In order to examine this, the $J_{\rm rms}$ of different isotopes of palladium, xenon, and barium in the ^{252}Cf(SF) from Refs. [7,20,21] are plotted in Fig. 3. The higher $J_{\rm rms}$ of ^{111}Pd, ^{140}Xe, and ^{142}Ba having a deformed 66-n or 88-n shell in their fragment stage can be clearly seen from Fig. 3. The above observations indicate that fragment angular momentum depends on deformation at scission. The effect of deformation can also be observed from the higher $J_{\rm rms}$ for the fission products in the rare earth region having permanent ground state deformation [7,14,21], e.g., ^{148}Pm in ^{234,236}U* [14], ^{154}Pm in ^{250}Cf* [21], as well as ^{146,148,150}Ce, ^{152,154}Nd, and ^{158}Sm in ^{252}Cf(SF) [7], respectively. The higher angular momentum of the super-deformed fragments such as ^{144,146}Ba and ^{104}Mo in ^{252}Cf(SF) observed from γ-γ-γ coincidence measurements [8] confirms the effect of deformation on fragment angular momentum. Further, the decrease of fragment angular momentum with increasing kinetic energy for various fission products in thermal neutron induced fission of ^{233}U, ^{235}U, and ^{239}Pu from the recoil mass separated data [9–11] also supports the above fact. From the above discussion it is clear that the angular momentum is related to the fragment deformation at scission in addition to the single particle spin contribution. In view of this, the deformation parameter (β) of the fission fragments in the six even-odd fissioning systems was calculated from the experimentally determined $J_{\rm rms}$ values and kinetic energy data as done in the earlier work [20–22].

Assuming statistical equilibrium among the various collective degrees [1,7], the rms angular momentum ($J_{\rm rms}$) of the fragment is related to the moment of inertia (I) and the temperature (T) as [7]

$$J_{\rm rms} = 2IT/\hbar^2. \tag{1}$$

The moment of inertia (I) is related to the fragment excitation energy (E^*) as [17]

$$I = I_{\rm rig}[1 - 0.8\exp(-0.693E^*/5)] \quad \text{and} \quad E^* = aT^2, \tag{2}$$

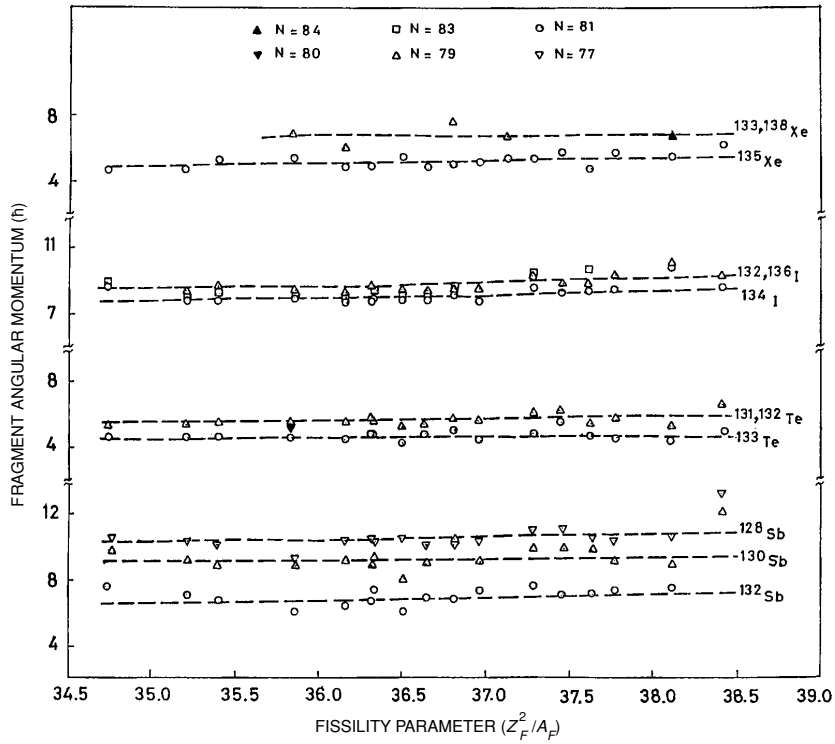

FIG. 2. Effect of the spherical 82-neutron shell on the fragment angular momentum in various fissioning systems.

where $I_{\rm rig}$ is the rigid body moment of inertia of the fragment and a is the level density parameter taken as $a = A/8\,{\rm MeV}^{-1}$.

On the other hand, according to the prescission bending oscillation model [2,7] the average angular momentum ($J_{\rm av}$) of the fragment is given as [2]

$$J_{\rm av} = \sqrt{\pi}/(2\gamma) - 0.5,\ J_{\rm av} = \sqrt{\pi}/2J_{\rm rms}, \tag{3}$$

where γ is the bending mode oscillation amplitude or the angular positional uncertainty. γ is approximately related [7] to the neck radius (c) and the semimajor axis (z) at deformation (β) as [39]

$$\gamma = c/z,\ z = R(\beta)[1 + (\sqrt{5}/4\pi)\beta], \tag{4}$$

where $R(\beta)$ is the radius considering volume conservation given as

$$R(\beta) = R[1 - (15/16\pi)\beta^2 + 0.25(5/4\pi)^{3/2}\beta^3]^{-1/3}. \tag{5}$$

The neck radius, c, can also be related to the deformation parameter (β) through the scission point distance (D) and thus with the fragment kinetic energy (E_K^f) on the basis of the condition [20] of equality of the Coulomb and nuclear forces at the scission point as

$$Z(Z_F - Z)e^2/D^2 = 2\pi c^2\Omega/\lambda,\ D = z_1 + z_2 \tag{6}$$

$$E_K^f = (1 - A/A_F)E,\ E = Z(Z_F - Z)e^2/D, \tag{7}$$

where Ω and λ are the coefficient and range of the attractive nuclear force, usually taken as 1.107 MeV/fm^2 and 0.68 fm, respectively [40]. A_F and Z_F are the mass and charge of the fissioning nucleus; E is the total kinetic energy.

From the above equations it is seen that the calculation of the deformation parameter (β) for a given fragment from its $J_{\rm rms}$ value requires the knowledge of either T or c for the corresponding split. It was shown by Wilkins *et al*. [41] that fragment deformation (β) (0.95 times the Bohr-Mottelson parameter) varies up to 1.0 for various fragments, and T might be 1.0 MeV. On the other hand, Wilhelmy *et al*. [7] showed the c value to be in the range of 1.0 to 1.6 fm. In view of these considerations the $J_{\rm rms}$ for each fragment was calculated within $1\hbar$ of the experimental value using both the statistical correlation and bending oscillation models by varying β from 0.001 to 1.0, T from 0.3 to 2.0 MeV, and c from 0.5 to 2.0 fm, respectively. Thus the c and T values resulting in

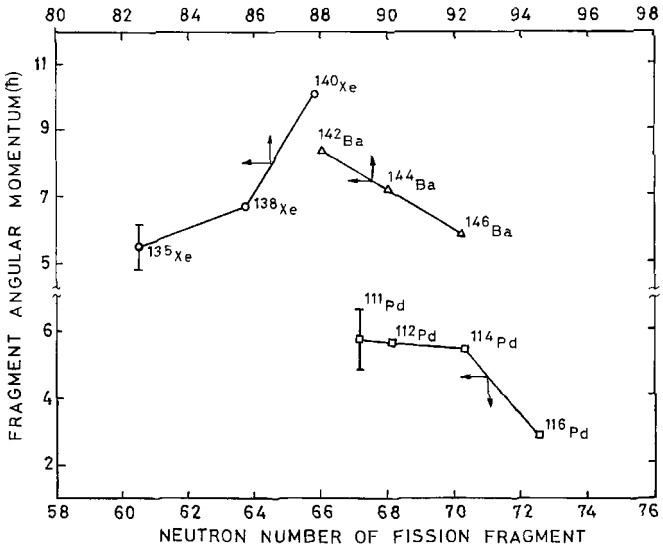

FIG. 3. Effect of deformed 88- and 66-neutron shell on the fragment angular momentum in ^{252}Cf(SF). The arrows indicate the corresponding axis.

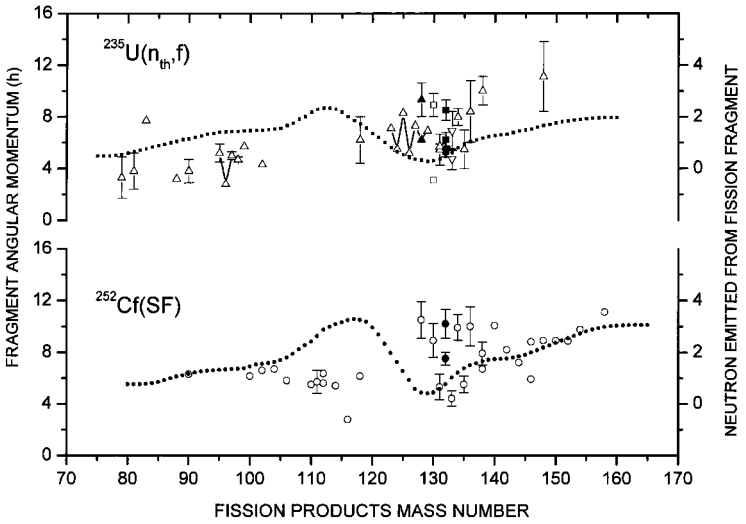

FIG. 4. Plot of fragment angular momentum and average neutron number emitted as a function of mass number of different fission products in ^{235}U($n_{\rm th}$, f) and ^{252}Cf(SF). (The dotted line represents the neutron emission curve, and the other symbols are for the fragment angular momentum. In ^{235}U($n_{\rm th}$, f) the triangles joined with the solid line are for $^{95-98}$Y and $^{123-129}$In. The filled triangles are for ^{128}In and ^{128}Sb. The open squares are for ^{130}Sn and ^{130}Sb. The filled squares are for ^{132}Sb, ^{132}Te, and ^{132}I. The inverted triangles are for ^{133}Te and ^{133}Xe. In ^{252}Cf(SF) the filled circles are for ^{132}Sb and ^{132}I).

the approximate fragment $J_{\rm rms}$ for each β value were deduced. Subsequently for each value of c, the kinetic energy (E) for that particular split was calculated using Eqs. (6) and (7). The appropriate values of β, T, and c for a fragment were then sorted out by comparing the calculated kinetic energy with the experimental one [42–48]. Since the kinetic energy for an individual split (i.e., as a function of charge for fixed mass) is not known, the experimental kinetic energy [42–48] for a particular mass corresponding to the average charge was used. In the fissioning systems the ^{241}Pu* and ^{245}Cm* experimental kinetic energies were not available. Therefore average E values from the fissioning systems ^{240}Pu* [46] and ^{242}Pu* [46] were used for ^{241}Pu*. Similarly for ^{245}Cm* the average E from the fissioning systems ^{244}Cm(SF) [47] and ^{246}Cm* [48] were used. The calculated deformation parameter (β), temperature (T), neck radius (c), and kinetic energy (E) along with the experimental values are given in Table I. In the case of odd-Z fragments the observed $J_{\rm rms}$ is likely to be influenced by the odd particle spin of the fragment itself. For such fragments, β values were calculated after correcting the fragment $J_{\rm rms}$ for the single particle spin ($\sim 2\hbar$) effect. The possible contribution due to postscission Coulomb torque was not considered as this contribution was evaluated to be low, within 1–2$\hbar$ (the same as the uncertainty on the experimental $J_{\rm rms}$ values), and since it does not enhance fragment spin consistently [2,7].

It can be seen from Table I that the β values calculated in the present work from $J_{\rm rms}$ in the spherical 82-n shell region are in close agreement with the β values obtained from the static scission point model [41] which confirms the validity of the present method. From Table I it can also be seen that the β values for the even-Z products and for the fragments having a closed 82-n shell are lower than the odd-Z products and fragments away from the shell region. This indicates the role of the deformation parameter on fragment angular momentum. The β values of different fragments in the even-odd fissioning systems (^{233}Th*, ^{233}U*, ^{239}U*, ^{239}Pu*, ^{241}Pu*, and ^{245}Cm*) from the present work are compared with those in the even-even fissioning systems [^{230}Th*, ^{234,236}U*, ^{240,242}Pu*, ^{244}Cm(SF), ^{246}Cm*, ^{250}Cf*, and ^{252}Cf(SF)] and odd-odd fissioning systems (^{238}Np* and ^{242}Am*) from earlier work [20–22]. It is observed that the β values of the even-Z fragments are more or less comparable in all the even-even, even-odd, and odd-odd fissioning systems. However, for the odd-Z fragments the β values are comparable only in the even-even and even-odd fissioning systems. In the odd-odd fissioning systems (^{238}Np* and ^{242}Am*) they are slightly higher than in their neighboring even-even fissioning systems [^{234,236}U*, ^{240,242}Pu*, ^{244}Cm(SF), and ^{246}Cm*] and even-odd fissioning systems (^{233,239}U*, ^{239,241}Pu*, and ^{245}Cm*), respectively. This is most probably due to the fact that odd-Z fragments in the odd-Z fissioning systems are more deformed at the cost of their even-Z complementary fragments. This shows the role of odd nucleon spin of the fissioning system when it is proton but not neutron, which may be due to the uncertainty of neutron evaporation.

B. Correlation of fragment angular momentum ($J_{\rm rms}$) with average neutron number and elemental yield

It can be seen from the present and earlier work [7–22] that maximum data are available in the mass region 128-138 in most of the fissioning systems except in ^{235}U($n_{\rm th}$, f) and ^{252}Cf(SF) where they are available over a wide mass range. In view of this in Fig. 4 the $J_{\rm rms}$ of various fission products are plotted as a function of their mass number in the fissioning systems ^{235}U($n_{\rm th}$, f) and ^{252}Cf(SF), respectively. The average number of emitted neutrons as a function of mass of the fission product from Ref. [35] is also shown in Fig. 4 for the above two fissioning systems. It can be seen from Fig. 4 that the $J_{\rm rms}$ values deduced either from independent isomeric yield ratios and/or from rotational band transition intensities do not show a sawtooth nature as a function of the fission products' mass number as do the prompt γ-ray and neutron emission. This does not mean that fragment deformation has no correlation with $J_{\rm rms}$ and prompt neutrons emitted from the fission fragment. The different behavior of $J_{\rm rms}$ values and prompt γ-ray or neutron emission is because the $J_{\rm rms}$ deduced from independent isomeric yield ratios and/or from rotational band transition intensities are for specific fission products with fixed mass and charge, whereas the γ-ray or neutron

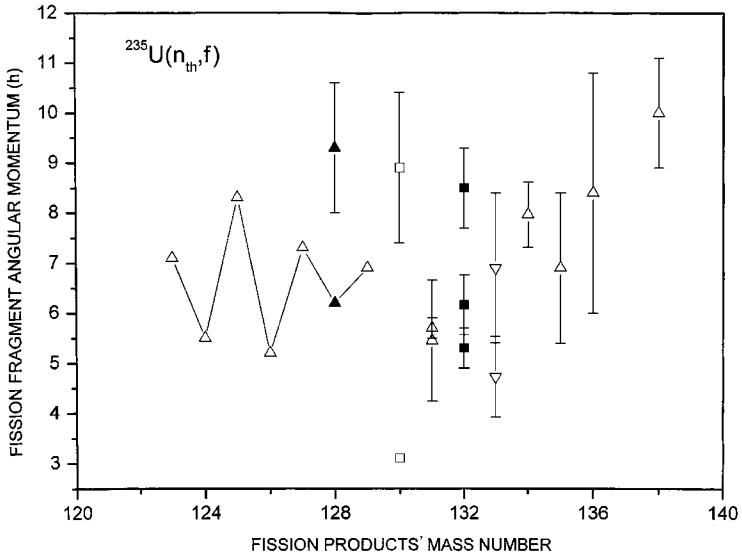

FIG. 5. Expanded portion of the plot of the fragment angular momentum as a function of mass number in the mass region 120–140 for the $^{235}U(n_{th}, f)$ reaction.

emission is for fixed masses with average charges. Thus the angular momentum deduced from γ-ray multiplicity [9] shows a sawtooth behavior like that of the neutron emission curve. Further, from Fig. 4 it can seen that different fission products with the same mass number (e.g., ^{128}In and ^{128}Sb, ^{130}Sn and ^{130}Sb, ^{132}Sb, ^{132}Te and ^{132}I, and ^{133}Te and ^{133}Xe) in $^{236}U^*$ have wide variations of J_{rms} values. This is clearly seen from Fig. 5, which is the expanded portion of Fig. 4 in the mass region 120–140 for the $^{235}U(n_{th}, f)$ reaction. The variation of J_{rms} values for the different fission products of the same mass number is due to the presence of the shell effect or odd-even effects, as explained in Section IIIA. For example, the lower J_{rms} of ^{132}Sb and ^{133}Te compared to those of ^{132}I and ^{133}Xe may be due to the nearer 82-n shell in the former products in their fragment stage. The lower J_{rms} of ^{128}In compared to those of ^{128}Sb may be also due to the nearer 82-n shell in the fragment stage of ^{128}In. On the other hand, the higher J_{rms} of ^{130}Sb and ^{132}I compared to those of ^{130}Sn and ^{132}Te may be due to odd-even effects. Similarly, the higher J_{rms} of the odd-A indium (^{123,125,127,129}In) and yttrium (^{95,97}Y) isotopes compared to those of the even-A indium (^{124,126,128}In) and yttrium (^{96,98}Y) isotopes in $^{235}U(n_{th}, f)$ may also be due to odd-even effects [9–11]. If one neutron emission takes place from the fission fragments in the above mass region, then the yttrium and indium isotopes are alternately even and odd. Thus the even-A fragments of yttrium and indium isotopes have higher J_{rms} values than their adjacent odd-A fragments. This may be due to the contribution of the individual spin from the odd neutron and odd proton of the fission fragment to the J_{rms} values. However, for even-Z elements, the J_{rms} values of so many adjacent isotopes are not available, except for ^{130,131}Sn and ^{131,132,133}Te in $^{235}U(n_{th}, f)$. In these cases, ^{131}Sn and ^{133}Te have spherical 82-n shells in their fragment stage and thus have lower J_{rms} values. So the neutron number in adjacent isotopes of tin and tellurium does not show its role prominently as in the case of adjacent yttrium and indium isotopes. It can also be seen from Fig. 4 that the J_{rms} values show a qualitative increasing trend with increasing mass number if one ignores the deviation of shell closure proximity and the odd-even effect. This finding can be explained by considering bending mode oscillation [2]. For heavy mass fragments it is expected that the uncertainty in angular position will be lower and the J_{rms} values will be higher, based on Eq. (4). In addition, the yield-weighted average angular momenta of heavy mass elements in fifteen even-Z fissioning systems from Table II and their elemental yields from literature [33–36] are plotted in Fig. 6. The angular momenta of heavy mass nuclides in the even-odd fissioning systems are from the present work, whereas in the even-even fissioning systems they are taken from earlier work [20,21]. From Fig. 6, an anticorrelation between angular momentum and elemental yield can be observed in all fifteen even-Z fissioning systems. This is because in low energy fission, the elemental yield is related to the intrinsic excitation energy [41], whereas the angular momentum is correlated to the deformation parameter of the fragment and thus to the deformation energy. The decrease of J_{rms} with a decrease of excitation energy or increase of kinetic energy [9–11] supports the correlation of the fragment angular momentum with the deformation parameter. Based on the scission point model [41], in the even-Z fissioning systems the odd-odd split has higher potential energy at scission resulting in a lower yield compared to their neighboring even-even split. As a consequence, an anticorrelation is observed between the angular momentum and the elemental yield. This indicates the coupling between collective and intrinsic degrees of freedom. Further, it can be seen from Fig. 6 that the odd-even effects on J_{rms} remain nearly the same or decrease slightly from Th to Cf, whereas the odd-even effects on elemental yield decrease significantly. This may be because of the linear dependence of the fragment angular momentum on deformation energy and a strong correlation between the proton odd-even effect and the intrinsic excitation energy [33,34,36]. From the above discussion, the following conclusions can be drawn:

1. The fragment angular momentum depends on nuclear structure effects such as spherical (50-p, 82-n) and deformed (66-n, 88-n) shell closure proximity. The higher J_{rms} of the

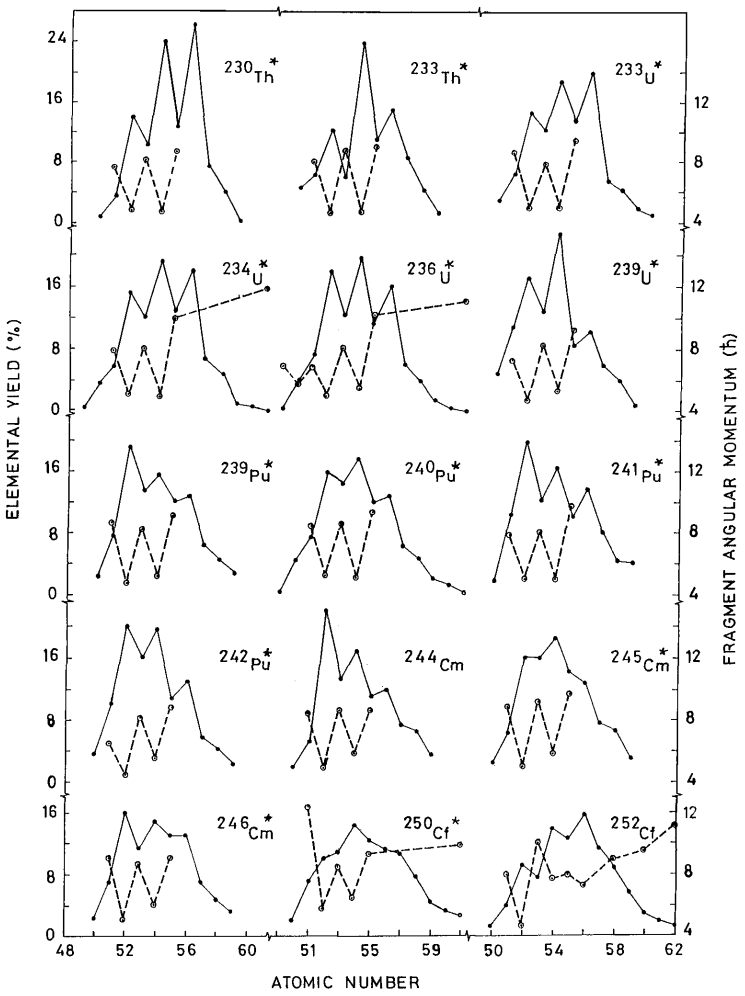

FIG. 6. Correlation of the yield-weighted average fragment angular momenta and the elemental yields in fifteen different even-Z fissioning systems. (The dashed line is for yield-weighted average fragment angular momenta and the solid line is for elemental yields.)

odd-Z or odd-A fragments are due to the single particle spin effects or the polarization of the even-Z core by the odd proton and/or neutron.

2. Deformation parameters (β) of the fission fragments deduced from their angular momenta and the experimental kinetic energy data are seen to be in good agreement with the theoretical values obtained from the static scission point model. The β values of the fragments with spherical shells and even-Z products are smaller than they are for the fragments with deformed shells, away from spherical shell and odd-Z products.
3. The $J_{\rm rms}$ of both even-Z and odd-Z products slightly increase with Z_F^2/A_F. This may be due to the increase of the Coulomb torque with Z_F^2/A_F. In addition, in all fissioning systems the $J_{\rm rms}$ of the fission fragments also increase with the mass number in spite of the fluctuation of odd-even effects and shell closure proximity. Thus, angular momenta of the fission fragments do not show a correlation with the average neutron emission curve.
4. In fifteen even-Z fissioning systems the yield-weighted average fragment angular momenta show an anticorrelation with elemental yields, probably due to the coupling between the collective and intrinsic degrees of freedom. However, the slight decrease of odd-even effects on fragment $J_{\rm rms}$ from Th to Cf may be due to a linear correlation with deformation energy. On the other hand, a drastic decrease of odd-even effects on elemental yield from Th to Cf may be due to a strong correlation with the intrinsic excitation energy.

ACKNOWLEDGMENTS

The authors express their sincere gratitude to Dr. V. K. Manchanda, Head of the Radiochemistry Division, BARC, and to Dr. A. V. R. Reddy, Head of the Nuclear Chemistry section, for their keen interest and encouragement in this work. Thanks are also due to Dr. R. H. Iyer, emeritus scientist, CSIR, for his valuable suggestions, and to the instrumentation group of the Radiochemistry Division, and S. V. Suryanarayan of the Nuclear Physics Division for their assistance.

[1] J. R. Nix and W. J. Swiatecki, Nucl. Phys. **71**, 1 (1965).
[2] J. O. Rasmussen, W. Norenberg, and H. J. Mang, Nucl. Phys. **A136**, 465 (1969).
[3] M. M. Hoffman, Phys. Rev. B, **133**, 714 (1964).
[4] V. M. Strutinskii, Sov. Phys. (JETP) **10**, 613 (1960).
[5] H. Nifenecker, C. Signarbieux, M. Ribrag, J. Poitou, and J. Matuszek, Nucl. Phys. **A189**, 285 (1972).
[6] P. Armbruster, H. Labus, and K. Reichelt, Naturforsch. A **26a**, 512 (1971); F. Plesonton, R. L. Ferguson, and H. W. Schmitt, Phys. Rev. C **6**, 1023 (1972).
[7] J. W. Wilhelmy, E. Cheifetz, R. C. Jared, S. G. Thompson, H. R. Bowman, and J. R. Rasmussen, Phys. Rev. C **5**, 2041 (1972).
[8] G. M. Ter-Akopian, J. H. Hamilton, Yu. Ts. Oganessian, A. V. Danniel, J. Kormicki, A. V. Ramayya, G. S. Popeko, B. R. S. Babu, Q.-H. Lu, K. Butler-Moore, W. -C. Ma, E. F. Jones, J. K. Deng, D. Shi, J. Kliman, M. Morhac, J. D. Cole, R. Aryaeinejad, N. R. Johnson, I. Y. Lee, and F. K. McGowan, Phys. Rev. C **55**, 1146 (1997).
[9] J. P. Bocquet, F. Schussler, E. Monnand, and K. Sistemich, in *Proceedings of the Fourth IAEA Symposium on Physics and Chemistry of Fission, Julich, 1979* (IAEA, Vienna, 1980), Vol. II, p. 179.
[10] H. O. Denschlag, H. Braun, W. Faubel, G. Fischbach, H. Meixler, G. Paffarth, W. Porsch, M. Weis, H. Schrader, G. Siegert, J. Blachot, Z. B. Alfassi, H. N. Erten, T. Izak-biran, T. Tamai, A. C. Wahl., and K. Wolfsberg, in *Proceedings of the Fourth IAEA Symposium on Physics and Chemistry of Fission, Julich, 1979* (IAEA, Vienna, 1980), Vol. II, p. 153.
[11] H. O. Denschlag, in *Proceedings of the Symposium on Radiochemistry and Radiation Chemistry* (IGCAR, Kalpakkam, India, 1989), p. IT-10.
[12] G. Rudstam, P. Aagaard, B. Ekstrom, E. Lund, H. Gokturk, and H. U. Zwicky, Radiochim. Acta **49**, 155 (1990).
[13] D. G. Sarantities, G. E. Gordon, and C. D. Coryell, Phys. Rev. **138**, B353 (1965).
[14] D. C. Aumann, W. Guckel, E. Nirschl, and H. Zeising, Phys. Rev. C **16**, 254 (1977).
[15] T. Datta, S. P. Dange, A. G. C. Nair, S. Prakash, and M. V. Ramaniah, Phys. Rev. C **25**, 358 (1982).
[16] G. P. Ford, K. Wolfsberg, and B. R. Erdal, Phys. Rev. C **30**, 195 (1984).
[17] I. Fujiwara, N. Imanishi, and T. Nishi, J. Phys. Soc. Jpn. **51**, 1713 (1982); N. Imanishi, I. Fujiwara, and T. Nishi, Nucl. Phys. **A263**, 141 (1976).
[18] B. S. Tomar, A. Goswami, S. K. Das, T. Datta, S. Prakash, and M. V. Ramaniah, Radiochim. Acta **39**, 1 (1985); B. S. Tomar, A. Goswami, A. V. R. Reddy, S. K. Das, S. B. Manohar, and S. Prakash, Radiochim. Acta **55**, 173 (1991).
[19] S. P. Dange, H. Naik, T. Datta, R. Guin, S. Prakash, and M. V. Ramaniah, J. Radioanal. Nucl. Chem. Lett. **108**, 269 (1986); S. P. Dange, H. Naik, T. Datta, A. V. R. Reddy, S. Prakash, and M. V. Ramaniah, Radiochim. Acta **39**, 127 (1986).
[20] T. Datta, S. P. Dange, S. K. Das, S. Prakash, and M. V. Ramaniah, Z. Phys. A: Atoms and Nuclei **A324**, 81 (1986); H. Naik, R. J. Singh, and R. H. Iyer, Radiochim. Acta **92**, 1 (2004).
[21] H. Naik, S. P. Dange, R. J. Singh, T. Datta, Nucl. Phys. **A587**, 273 (1995); H. Naik, T. Datta, S. P. Dange, P. K. Pujari, S. Prakash, and M. V. Ramaniah, Z. Phys. A: Atoms and Nuclei **A331**, 335 (1988).
[22] H. Naik, S. P. Dange, and R. J. Singh, Eur. Phys. J. A **7**, 377 (2000).
[23] K. Flynn, Argonne National Laboratory Report ANL 75-25, 1975 (unpublished).
[24] E. Browne and R. B. Firestone, in *Table of Radioactive Isotopes*, edited by V. S. Shirley (Wiley & Sons, New York, 1986).
[25] J. Blachot and Ch. Fiche, Ann. Phys. (Paris) **6**, 3-218 (1981).
[26] H. N. Erten, A. Grutter, E. Rossler, and H. R. von Gunten, Phys. Rev. C **25**, 2519 (1982).
[27] T. Izak-Biran and S. Amile, Phys. Rev. C **16**, 266 (1977).
[28] R. Hentzschel and H. O. Denschlag, Radiochim. Acta **50**, 1 (1990).
[29] E. Dobreva and N. Nenoff, J. Radioanal. Nucl. Chem. Articles **81**, 29 (1984); S. J. Balestrini and L. Forman, Phys. Rev. C **10**, 1872 (1974); K. Wolfsberg, J. Inorg. Nucl. Chem. **37**, 1125 (1975).
[30] R. H. Iyer, H. Naik, A. K. Pandey, P. C. Kalsi, R. J. Singh, A. Ramaswami, and A. G. C. Nair, Nucl. Sci. Eng. **135**, 227 (2000); H. Naik, A. G. C. Nair, P. C. Kalsi, A. K. Pandey, R. J. Singh, A. Ramaswami, and R. H. Iyer, Radiochim. Acta **75**, 69(1996).
[31] M. Haddad, J. Crancon, G. Lhospice, and M. Asghar, Radiochim. Acta **46**, 23 (1989).
[32] M. Haddad, J. Crancon, G. Lhospice, and M. Asghar, Nucl. Phys. **A481**, 333 (1988).
[33] H. Naik, R. J. Singh, and R. H. Iyer, Eur. Phys. J. A **16**, 495 (2003); H. Naik, R. J. Singh, and R. H. Iyer, J. Phys. G: Nuclear Particle Physics **30**, 107 (2004).
[34] H. Naik, S. P. Dange, R. J. Singh, and S. B. Manohar, Nucl. Phys. **A612**, 143 (1997).
[35] A. C. Wahl, At. Data Nucl. Data Tables **39**, 1 (1988).
[36] J. P. Bocquet and R. Brissot, Nucl. Phys. **A502**, 213c (1989).
[37] J. R. Huizenga, and R. Vandenbosch, Phys. Rev. **120**, 1305 (1960); W. L. Hafner, J. R. Huizenga, and R. Vandenbosch, Argonne National Laboratory Report ANL-6662, 1962 (unpublished).
[38] V. A. Madsen and V. R. Brown, Phys. Rev. Lett. **52**, 176 (1984); V. A. Madsen, V. R. Brown, and J. D. Anderson, Phys. Rev. C **12**, 1205 (1975).
[39] H. Schultheis and R. Schultheis, Phys. Rev. C **18**, 1317 (1978).
[40] K. T. R. Davies, A. J. Sierk, and J. R. Nix, Phys. Rev. C **13**, 2385 (1976).
[41] B. D. Wilkins, E. P. Steinberg, and R. R. Chasman, Phys. Rev. C **14**, 1832 (1976).
[42] W. Holubarsch, E. Pfeiffer, and F. Goennenwein, Nucl. Phys. A **171**, 631 (1971); N. P. Dyachenko, B. D. Kuzminov, V. V. Malinovskii, V. F. Mitrofankov, A. I. Sergachev, S. M. Solovev, and P. S. Soloshenkov, Sov. J. Nucl. Phys. **30**, 469 (1979).
[43] M. Asghar, F. Caitucoli, B. Leroux, P. Perrin, and G. Barreau, Nucl. Phys. **A368**, 328 (1981).
[44] V. G. Vorob'eva, B. D. Kuz'minov, A. I. Sergachev, and M. Z. Tarasko, Sov. J. Nucl. Phys. **9**, 175 (1969); M. J. Bennett and W. E. Stein, Phys. Rev. **156**, 1277 (1967).
[45] M. Asghar, F. Caitucoli, B. Leroux, M. Maurel, P. Perrin, and G. Barreau, Nucl. Phys. **A368**, 319 (1981).
[46] J. N. Neiler, F. J. Walter, and H. W. Schmitt, Phys. Rev. **149**, 894 (1966).

[47] I. D. Alkhazov, O. I. Kostochkin, S. S. Kovalenko, L. Z. Malkin, K. A. Petrzhak, and V. I. Shpakov, Sov. J. Nucl. Phys. **11**, 281 (1970); Yu. A. Barashkov, Yu. A. Vasil'ev, A. N. Maslov, E. S. Pavlovskii, M. K. Sareava, L. V. Sidorov, V. M. Surin, and P. V. Toropov, Sov. J. Nucl. Phys. **13**, 668 (1971).

[48] J. P. Unik, J. E. Gindler, L. E. Glendenin, K. F. Flynn, A. Gorski, and R. K. Sjoblom, in *Proceedings of the Third IAEA Symposium on Physics and Chemistry of Fission, Rochester, NY, 1973* (IAEA, Vienna, 1974), Vol. II, p. 19.